frontiers in Physics

ORIGINAL RESEARCH
published: 30 October 2020
doi: 10.3389/fphy.2020.579168

Quantification of Visco-Elastic Properties of a Matrigel for Organoid Development as a Function of Polymer Concentration

Mads Borries[1†], *Younes Farhangi Barooji*[1†], *Siham Yennek*[2], *Anne Grapin-Botton*[2], *Kirstine Berg-Sørensen*[3,4#] *and Lene B. Oddershede*[1*]

[1] *Niels Bohr Institute, University of Copenhagen, Copenhagen, Denmark,* [2] *The Novo Nordisk Foundation Center for Stem Cell Biology, University of Copenhagen, Copenhagen, Denmark,* [3] *Department of Physics, Technical University of Denmark, Kongens Lyngby, Denmark,* [4] *DTU Health Technology, Lyngby, Denmark*

The biophysical properties of polymer based gels, for instance the commonly used Matrigel, crucially depend on polymer concentration. Only certain polymer concentrations will produce a gel optimal for a specific purpose, for instance for organoid development. Hence, in order to design a polymer scaffold for a specific purpose, it is important to know which properties are optimal and to control the biophysical properties of the scaffold. Using optical tweezers, we perform a biophysical characterization of the biologically relevant Matrigel while systematically varying the polymer concentration. Using the focused laser beam we trace and spectrally analyze the thermal fluctuations of an inert tracer particle. From this, the visco-elastic properties of the Matrigel is quantified in a wide frequency range through scaling analysis of the frequency power spectrum as well as by calculating the complex shear modulus. The viscoelastic properties of the Matrigel are monitored over a timespan of 7 h. At all concentrations, the Matrigel is found to be more fluid-like just after formation and to become more solid-like during time, settling to a constant state after 1–3 h. Also, the Matrigel is found to display increasingly more solid-like properties with increasing polymer concentration. To demonstrate the biological relevance of these results, we expand pancreatic organoids in Matrigel solutions with the same polymer concentration range and demonstrate how the polymer concentration influences organoid development. In addition to providing quantitative information about how polymer gels change visco-elastic properties as a function of polymer concentration and time, these results also serve to guide the search of novel matrices relevant for organoid development or 3D cell culturing, and to ensure reproducibility of bio-relevant Matrigels.

Keywords: optical trapping, viscoelasticity, polymer network, complex shear moduli, organoid development

OPEN ACCESS

Edited by:
Halina Rubinsztein-Dunlop, The University of Queensland, Australia

Reviewed by:
Khoi Tan Nguyen, Vietnam National University, Vietnam
Jianming Wen, Kennesaw State University, United States

****Correspondence:***
Lene B. Oddershede
oddershede@nbi.ku.dk

[†]These authors have contributed equally to this work

[#]Present address:
Kirstine Berg-Sørensen
Department of Health Technology, Technical University of Denmark, Kgs Lyngby, Denmark

Specialty section:
This article was submitted to Optics and Photonics, a section of the journal Frontiers in Physics

Received: *01 July 2020*
Accepted: *22 September 2020*
Published: *30 October 2020*

Citation:
Borries M, Barooji YF, Yennek S, Grapin-Botton A, Berg-Sørensen K and Oddershede LB (2020) Quantification of Visco-Elastic Properties of a Matrigel for Organoid Development as a Function of Polymer Concentration. Front. Phys. 8:579168. doi: 10.3389/fphy.2020.579168

INTRODUCTION

Cells in an organism are surrounded by a matrix, often made of biopolymers, whose physical properties dramatically influence cell behavior. For instance, the visco-elastic properties of the extracellular matrix (ECM) has been shown to play an important role in fundamental cellular processes such as cell migration [1, 2], proliferation [3–5], and differentiation [6–8], as well as for the spreading of cancerous cells [5, 9, 10]. For this reason, much effort has been put into developing physics-based tools, experimental and theoretical, to enable characterization of the biophysical properties of polymer solutions. Atomic force microscopy (AFM) and shear rheology are two common experimental techniques which allow for quantification of the elastic properties of the ECM [11, 12]. However, both methods still struggle to measure the stiffness changes of the ECM during imaging of cells in culture media and none of them have the ability to measure deep inside organisms or tissue in a non-invasive manner. Optical tweezers and video-microscopy are two other techniques, which has proven capable of quantifying visco-elastic properties, also inside living cells and organisms, through passive monitoring of an optically trapped tracer particle. These methods have the advantage that they provide both the elastic and viscous responses of a polymer matrix over a large frequency range, including the range relevant for polymer dynamics [13, 14].

Cellular development can be influenced, or controlled, by proper matrix choice. This is instrumental for the development of organoids, which are 3D cell models, derived from a few cells, which allow for *in vitro* expansion of an organ for potential medical usage. Matrigel is the most commonly used polymer matrix for successful organoid development. In this paper, we use Matrigel as a biologically relevant polymer matrix with the purpose of systematically investigating how the physical properties of the polymer matrix change as a function of polymer concentration. Thereby, we continue work which was sparked by investigating the elastic properties of actin network by MacKintosh et al in 1995 [15]. More than 1800 peptides have been identified in Matrigel, however, the main components are Laminin (~ 60%), Collagen IV (~ 30%) and entactin/nidogen (~ 8%), while the remaining ~ 2% consists of a wide range of macromolecules, including proteoglycans. A major difference in protein composition, when comparing the basal lamina or Matrigel to another ECM as, e.g., the connective tissue, is a higher proportion of Laminin compared to Collagen IV. Laminin is a macromolecule with structural functions that especially can withstand tensile forces, while Collagen IV assembles into very large, stiff structures. As a result of this, Matrigel has much more tensile resilience than compressive resilience. Its physical properties then correlate with its role as an element that for example, connects skin cells to connective tissue. One reason why Matrigel is particularly relevant is that mixtures of Matrigel and media have resulted in unprecedented achievements in organoid growth in 3-dimensional structures [16, 17].

Here, we systematically quantify the viscoelastic properties of Matrigel preparations at different polymer concentrations using a passive optical tweezers based method which can be carried out non-invasively during confocal imaging of the sample. These results have interest also for other types of polymeric solution where it is an outstanding question how the viscoelastic properties depend on the polymer concentration. It is also demonstrated how the physically different matrices result in different growth of embedded organoids.

MATERIALS AND METHODS

Optical Setup

An overview of the optical tweezers based setup used for the experiments is provided in **Figure 1**. The optical trap is constructed from an infrared laser (1064 nm, Nd:YVO4, Spectra-Physics J20-BL10-106Q) directed into an inverted microscope (Leica, TCS SP5), equipped with a proper dicroic mirror. Both the laser and the microscope light are focused onto a sample placed in a sample holder through a water immersion objective (PL APO, NA = 1.2, 63X, w). The sample holder is placed on a movable piezo stage (Newport, XY Translation Stage Model M406), that is used to position the sample with respect to the focus of the optical trap. After interacting with the weakly trapped bead, the back-scattered light is collected by the condenser and imaged onto a Quadrant Photo Diode (QPD) (Hamamatsu, Si PIN photodiode S5981) in the back focal plane. In addition, the sample plane is imaged with a CCD camera (Imagesource, DFK 31AF03), monitoring the sample. The measurement output of the QPD, the raw data, consists of four voltages that are transformed into appropriate sums and differences linearly related to the position of the bead inside the trap [18, 19]. The laser was operated at 200–300 mW of which approximately 20% reached the sample plane.

Power Spectral Analysis Method

Optical tweezers exert a harmonic force, $F = \kappa x$, on a trapped bead, where κ is the spring constant and x is the distance from the bead's equilibrium position within the trap. For the bead sizes used here (~ 1μm), the spring constant is similar in the two directions perpendicular to the propagation of the laser light and smaller in the direction parallel to the laser light [20]. For a trapped bead with radius of r in a normal viscous fluid (e.g., water) with viscosity of η, power spectral analysis shows that the power spectrum $P(f)$ at frequency f is ideally given by [21, 22].

$$P(f) = \frac{k_B T}{6\pi\eta r\beta^2} \frac{1}{\left(f_c^2 + f^2\right)}, \tag{1}$$

where f_c is the corner frequency, $k_B T$ is thermal energy and β is the calibration factor which is relating position measurement in Volts by the QPD to meters.

When the surrounding medium is a visco-elastic medium rather than a newtonian fluid, for frequencies well above the corner frequency of the trap, the power spectrum can be described by:

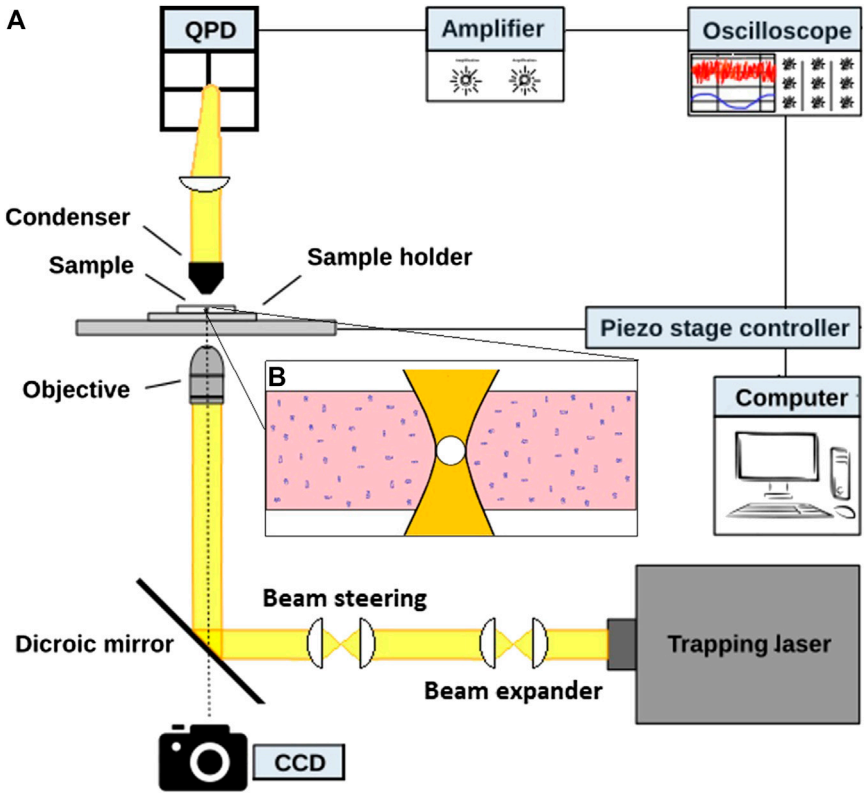

FIGURE 1 | Sketch of the setup. **(A)** 1,064 nm laser light is directed into an inverted microscope. The microscope objective focuses the laser onto a sample (b) placed on a movable piezo stage. After interacting with the sample, the back-scattered light is collected by a condenser and focused onto a Quadrant Photo Diode (QPD). A CCD camera monitors the sample. **(B)** Sketch of a sample containing Matrigel solution and an optically trapped tracer particle.

$$P(f) \propto f^{-(\alpha+1)}. \tag{2}$$

For tracer motion within a medium, the value of α relates to the behavior of the tracer particle as follows:

- $\alpha = 0$: The particle is **completely confined** by the surrounding medium.
- $0 < \alpha < 1$: The particle undergoes **sub-diffusion**, the lower the value of α, the more elastic the medium, and the closer to 1 the more viscous the medium.
- $\alpha = 1$: The particle performs **free diffusion** described as Brownian motion, and the surrounding medium is purely viscous.
- $\alpha > 1$: The particle undergoes **super-diffusion**, indicating that there are active processes and that particle movement is propelled by external forces.

Complex Shear Moduli

The frequency dependent complex shear modulus, $G(f) = G'(f) + iG''(f)$ can be found from the power spectral density and analysis of the response function of the trapped particle. The frequency dependent shear modulus, $G(f)$, has as its real part the elastic modulus, $G'(f)$, which describes the stored energy in the complex medium. Conversely, the imaginary part, the loss modulus, $G''(f)$, is a measure of the energy dissipated by deformation of the complex material. For a microparticle inside a viscoelastic medium, the Fourier transform of the stochastic thermal force, $F(f)$, and the Fourier transformed of the position of the particle, $x(f)$ are related through linear response theory [23],

$$x(f) = \gamma(f)F(f), \tag{3}$$

where $\gamma(f)$ is the compliance of the medium [24]. The medium compliance is a complex function which in turn is related to the viscoelastic modulus through the Generalized Stokes-Einstein relation,

$$G(f) = \frac{1}{6\pi r\gamma(f)}. \tag{4}$$

Thus, the different physical quantities are extracted as follows:

$$G'(f) = \frac{1}{6\pi r}\frac{\gamma'(f)}{\gamma'(f)^2 + \gamma''(f)^2} \tag{5}$$

$$G''(f) = -\frac{1}{6\pi r}\frac{\gamma''(f)}{\gamma'(f)^2 + \gamma''(f)^2} \tag{6}$$

$$\gamma''(f) = \frac{\pi f}{2k_B T}P(f) \tag{7}$$

$$\gamma'(f) = \frac{2}{\pi}\int_0^\infty \cos(2\pi f t)\mathrm{d}t \int_0^\infty \gamma''(f)\sin(\tilde{f}t)\mathrm{d}\tilde{f} \qquad (8)$$

where the last results follows from the Kramers-Kronig relation. This method is less challenging in comparison with active methods (oscillatory microrheology) [25], however, since the trap stiffness is not accounted for, the laser power should not be too high. And since the photodiode detection system may act as an unintended filter [26], the frequency span of the method lies between the corner frequency of trap and the filtering frequency of the photodiode, this frequency interval spanning several orders of magnitude and encompassing frequencies relevant for polymer dynamics. With these concerns accounted for, the frequency dependent viscoelastic characteristics of the medium can be determined as described above. The loss tangent, $\tan(\delta) = G''/G'$, relates to the overall behavior of the medium at the particular frequency, i.e., it describes the solid (or gel like) ($G''/G' < 1$)- or fluidlike ($G''/G' > 1$) behavior of the viscoelastic material.

Preparation of Matrigel Matrix and Sample Chamber

The major components of the ECM include water, proteins, and polysaccharides and different types of ECMs for cell culturing are commercially available, extracted from different types of tissue using different protocols [27–29]. ECM preparations of particular viscoelastic properties can be produced with different compositions by including a variety of proteins and biopolymers. Matrigel^R is a commercial ECM extracted from Engelbreth-Holm-Swarm mouse tumor cultures [30–33]. It is commonly used as a basement membrane matrix to support proliferation of stem cells while they remain in an undifferentiated state [34]. In addition, combinations of Matrigel and other ECM mixtures [35–37] are widely used as external matrix in culturing of 3D spheroids and organoids.

The Matrigel (Corning® Matrigel®, Growth Factor Reduced, Basement Membrane Matrix, Phenol Red-free, LDEV-free) was mixed with the nutrition medium Dulbecco's Modified Eagle Medium/Nutrient Mixture F-12 (DMEM) (Gibco™, GlutaMAX™, Additives: Sodium Pyruvate & Sodium Bicarbonate). The latter is a medium that has proven to support growth of several kinds of cells and organoids, such as the pancreas organoid, providing the addition of small quantities of additional growth factors [16, 17]. The nutrition medium contains a high concentration of amino acids, vitamins and glucose.

Sample chambers, with an inner height between 300 and 500 μm, were prepared by sticking two glass slides together using vacuum grease and the chambers were then cooled down. Frozen Matrigel was put on ice to slowly thaw. Since Matrigel becomes gel-like at above approximately 4°C, the temperatures of the solutions had to be kept between 0 and 4°C. The nutrition medium was cooled to the same temperature and mixed with a 0.96 μm polystyrene bead solution. Matrigel and the nutrition medium with polystyrene beads were mixed together using pipettes and injected in the sample chambers. The chambers were then sealed completely with vacuum grease. A chamber was placed on the microscope stage and beads were trapped to conduct a measurement once per hour during 7 h.

Trapping of Beads Inside Matrigel Sample

Immediately after sample preparation, the samples were taken to the optical tweezers setup. Beforehand the laser trap was calibrated to have its focus (**Figure 1B**) at the same axial position as the microscope objective's focus and to have its lateral center in the center of the field of view of the objective. At this position, the tracer beads were physically trapped in a harmonic potential. Before turning on the laser, the dispersed beads were localized and positioned in the center of the microscope objective's focus point. The laser was then activated, it was operated at relatively low laser powers and the bead was hence trapped in a weak harmonic potential. While the bead was trapped and performing thermal fluctuations, its positions were recorded by QPD. In each chamber, for each concentration and at each point in time, five beads were trapped. And for each bead, three microrheology measurements were conducted.

Mouse Pancreatic Organoid Culture and Measurement

Mouse pancreatic organoids were cultured as previously described [16, 17]. Briefly, pancreatic progenitors were isolated from the dorsal pancreatic bud of a litter of mouse embryos at embryonic day (e)10.5, typically 10 embryos. The epithelial part of the bud was dissected from the surrounding mesenchyme and remaining digestive tract with microneedles, dissociated to single cells and small clusters using Trypsin 0.5% (about 5,000 cells from 10 pooled embryos) and mixed with growth factor-depleted Matrigel on ice. Drops of 8 μl of the cell:Matrigel mixture were deposited on culture plates, allowed to gel at 37°C and cultured in organoid medium [16, 17] for 7 days. In these conditions clusters of cells proliferate and self-organize to form organoids. Three concentrations of Matrigel were tested: 75%, 50%, and 25%. Images of organoid cultures were acquired after day 1, day 2, day 4, day 5 and day 7 in culture on a Leica AF6000 (HCX PL FLUOTAR 10x/0.30 Ph1 Dry, Leica DFC365 FX camera) in such a way that every single organoid could be tracked over time. Organoid area was measured over time using the freehand selection tool on ImageJ. The radius (r) of the measured areas was calculated assuming a spherical shape, and organoid growth was determined by plotting r^3 of organoids over time, normalized to r^3 of the same organoid at day 1. This analysis corrects for the dependency of the final size of the organoid on the initial seed size observed at day 1.

To quantify the branching of the growing organoids, the focus plane of the objective yielding the largest area for each organoid was used to determine the area of individual organoids. At this plane, the length of the outer membrane surrounding the entire organoid, the perimeter, was quantified by Fiji routines. The ratio perimeter^2/area was calculated for each organoid in order to have a dimensionless measure of branching, that is, size-independent.

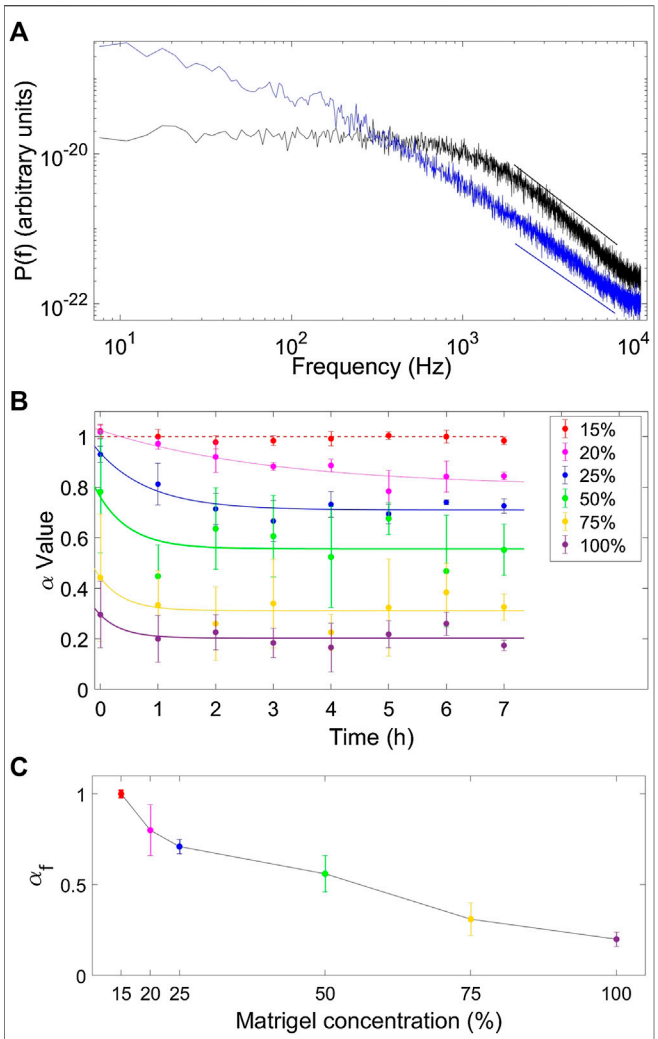

FIGURE 2 | Determination of scaling properties and evaluation of how these change as a function of time and concentration. **(A)** Power spectrum of an optically trapped particle in water (black, $\alpha = 1$) and in a Matrigel mixture (ratio 75% medium to 25% matrigel) (blue, $\alpha = 0.71$) 7 h after preparation of the sample. The straight lines show fits of **Eq. 2** to data, fits were carried out on data blocked as described in refs. 38 and 39. **(B)** Values of α as a function time for tracer particles embedded in different concentrations of matrigel solution (15% red, 20% magenta, 25% blue, 50% green, 75% orange, and pure Matrigel solution (100%) purple). Solid lines show exponential fits to the experimental data which indicate that α reaches an asymptotic value, α_f, after a few hours. **(C)** The value of α_f decreases with Matrigel concentration: α_f = 1.00 ± 0.02 for 15% Matrigel, α_f = 0.80 ± 0.14 for 20% Matrigel, α_f = 0.71 ± 0.04 for 25% Matrigel, α_f = 0.56 ± 0.10 for 50% Matrigel, α_f = 0.31 ± 0.09 for 75% Matrigel, and α_f = 0.20 ± 0.04 for 100% Matrigel.

RESULTS AND DISCUSSION

Viscoelastic Properties of the Matrigel Changes as a Function of Time and Concentration

To characterize the viscoelastic properties of each sample, we retrieved α by fitting **Eq 2** to the experimentally obtained power spectral data (PSD) in the frequency range 2000 Hz < f < 8,000 Hz. The miminum frequency, 2 kHz, was chosen well above the corner frequency, f_c, in order to avoid the frequency interval where the optical trap had a confining effect. The maximum frequency, 8 kHz, was chosen well below the cut-off frequency, f_{3dB}, of the quadrant photodiode [26].

Figure 2A shows two examples of the PSD as a function of frequency on a double-log plot for a trapped bead in water (a purely viscous liquid, black in **Figure 2A**) and in a 25% Matrigel solution (a viscoelastic medium, blue in **Figure 2A**). The two PSDs in **Figure 2A**) illustrate the difference in scaling properties of a tracer particle embedded in a purely viscous media as opposed to embedment in a viscoelastic media. Beads moving in a mixture with only 15% Matrigel solution behave as if they had been in a normal Newtonian liquid like water as their motion was characterized by $\alpha \sim 1$. Higher concentrations of Matrigel (20%, 25%, 50%, 75%, and 100%) lead to values of α significantly less than 1, indicating that the mixture of Matrigel and nutrition medium for these concentrations of Matrigel have both viscous and elastic properties.

Over time, the fitted value of α decreased from an initial value α_0 to a final asymptotic value, α_f (see **Figure 2B**). This temporal behavior of α was well fitted by an exponential function, $\alpha(t) = \alpha_0 e^{-t/\tau} + \alpha_f$, as seen in **Figure 2B**), where the parameter τ is a

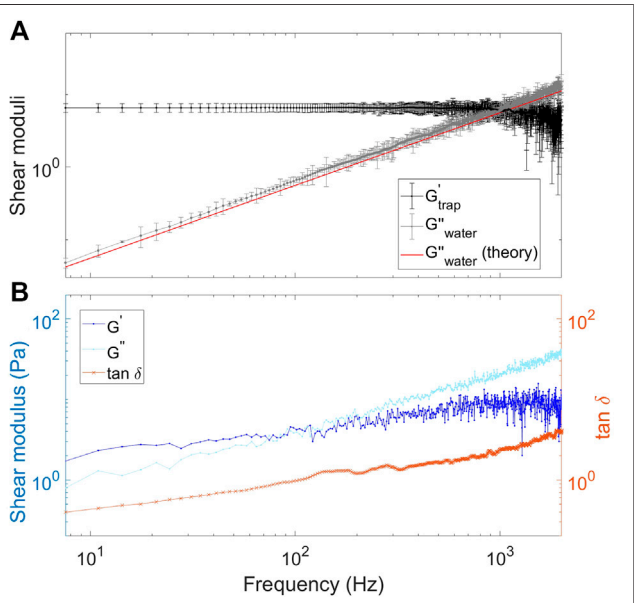

FIGURE 3 | Extraction of complex shear moduli for tracer particles in water or Matrigel solutions. **(A)** Extracted complex shear moduli for a bead trapped in water. The black symbols and black line show the storage modulus. The gray symbols and gray line show the loss modulus, the results being in agreement with theory (red line) for a viscous liquid. **(B)** Extracted storage modulus, G'(blue), and loss modulus, G''(light-blue), for a bead trapped in a Matrigel solution (75 medium:25 Matrigel). Both G' and G'' increase as a function frequency. At low frequencies, the Matrigel solution exhibits solid-like behavior. At around 100 Hz the loss modulus equals the storage modulus, and at frequencies higher than 100 Hz the solution exhibits liquid like behavior. The orange line shows the loss tangent which is below or above 1 for solid- or liquid-like behavior, respectively.

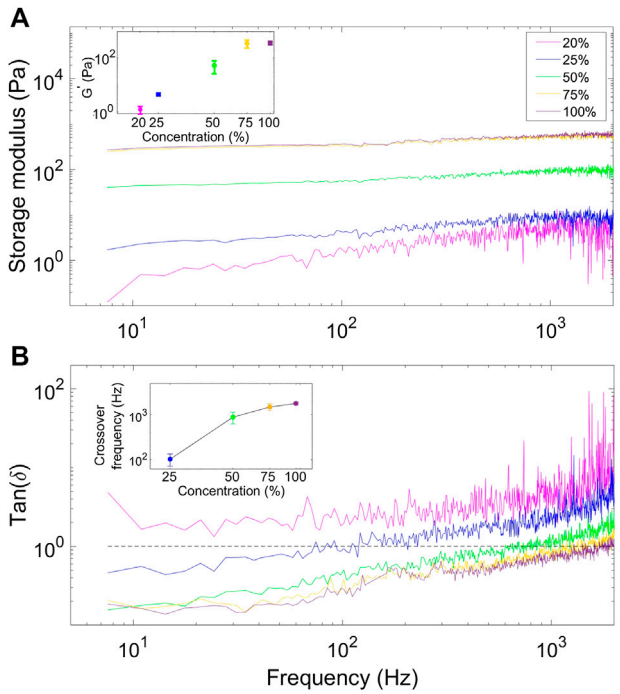

FIGURE 4 | Analysis of how the elastic properties of the matrix change with polymer concentration. **(A)** Storage moduli of mixtures with different Matrigel concentrations (20% magenta, 25% blue, 50% green, 75% orange, and pure Matrigel solution (100%) purple). At all frequencies, the storage moduli increase with Matrigel concentration. The inset shows the value of the storage modulus at f = 100 Hz as a function of Matrigel concentration. **(B)** Loss tangents as a function of frequency for different Matrigel concentrations. The insert shows the value of the crossover frequency, the frequency at which $\tan(\delta) = 1$, as a function of concentration. The cross-over frequency marks the frequency at which the solution shifts from solid- to liquid-like behavior. The data were collected 7 h after the sample preparation.

relaxation time. The asymptotic value of the exponent, α_f, decreases as the concentration of Matrigel increases, thus indicating that the polymeric mixture becomes more rigid as a function of time (**Figure 2C**).

Complex Shear Moduli of Matrigel Change With Concentration

The viscoelastic properties of the Matrigel were also investigated through their complex shear moduli as described in Methods, however, with the extra consideration that the contribution from the optical trap should also be considered. For a particle trapped inside the medium, $G'(f)$ as calculated directly from the data is an effective modulus which contains both the contribution from the elastic modulus of the surrounding medium and the contribution from the trap [24], G'_{trap}. Therefore, the contribution from the trap should be subtracted from the effective value calculated from the raw data. To determine the storage modulus of the trap, we extracted the elastic modulus for a bead trapped in water as a purely viscous medium, otherwise following an identical procedure. The resulting storage modulus of the trap ($G'_{\mathrm{trap}} = 6.57 \pm 0.9\,Pa$) is shown in **Figure 3A**). The experimental data shows the expected behavior of the loss modulus for water; in particular, we observe that $G''_{\mathrm{trap}}(f)$ scales with $\alpha = 1$ as expected for a purely viscous medium where $G'' = 2\pi\eta f$ (**Figure 3A**). The apparent decrease in the shear moduli for the highest frequencies is an artifact resulting from the finite experimental maximum frequency when evaluating the integrals in **Eq. 8**, as also described in ref. 40.

Once the storage moduli of water are known, the shear moduli corresponding to the Matrigel solution can be extracted. As discussed above, in a solution with a 15% concentration of Matrigel, the bead experiences a medium with properties very similar to water, see also **Figure 2B**), which is probably due to the very low concentration of polymers. For a 20% Matrigel mixture, the loss modulus dominates the storage modulus in the entire measured frequency interval, thus implying that the solution has a dominantly liquid like behavior ($\tan(\delta) > 1$). The mixtures with 25% Matrigel concentration and higher show solid like behavior ($\tan(\delta) < 1$) at low frequencies whereas the behavior changes to a liquid-like phase ($\tan(\delta) > 1$) after the crossover point ($G'' = G'$), see **Figure 3B**).

Figure 4A) demonstrates that the storage modulus of Matrigel mixtures increases with Matrigel concentration over the entire frequency range, the inset in a) shows the value of the loss modulus at f = 100 Hz as a function of concentration. The same conclusion can be drawn from inspecting the loss tangent as a function of frequency for different Matrigel concentration; the loss tangent clearly increases with Matrigel concentration over the entire frequency range (**Figure 4B**). The inset in **Figure 4B**) shows the cross over frequency, i.e., the frequency at which $\tan(\delta) = 1$, as a function of Matrigel concentration, further cementing the observation that the higher the polymer concentration, the more solid-like the matrix.

Effect of Matrigel Concentration on Organoid Expansion

To test whether variations of the mechanical properties of a Matrigel polymer matrix affects pancreas organoid growth and branching patterns, we seeded pancreatic progenitors isolated from e10.5 embryos in Matrigel-based matrices with Matrigel concentrations in the range of 25–75%. As previously reported for 75% Matrigel, we observed that organoids grew during the entire 7-day period of observation. After day 4 they started to form bulges reminiscent of the branching patterns seen in the body (**Figure 5A**). While the growth (measured by normalized volume) was in the same range for organoids embedded in 25%, 50% or 75% Matrigel matrices (**Figure 5B**), their branching visually appeared greater in higher Matrigel concentrations (**Figure 5A**).

To further analyze the branching of organoids as a function of time, the morphology of the growing organoids was determined by measuring their area and perimeter. If the perimeter compared to area is large, compared that of a disk, there is a high degree of organoid branching. In order to have a measure for branching,

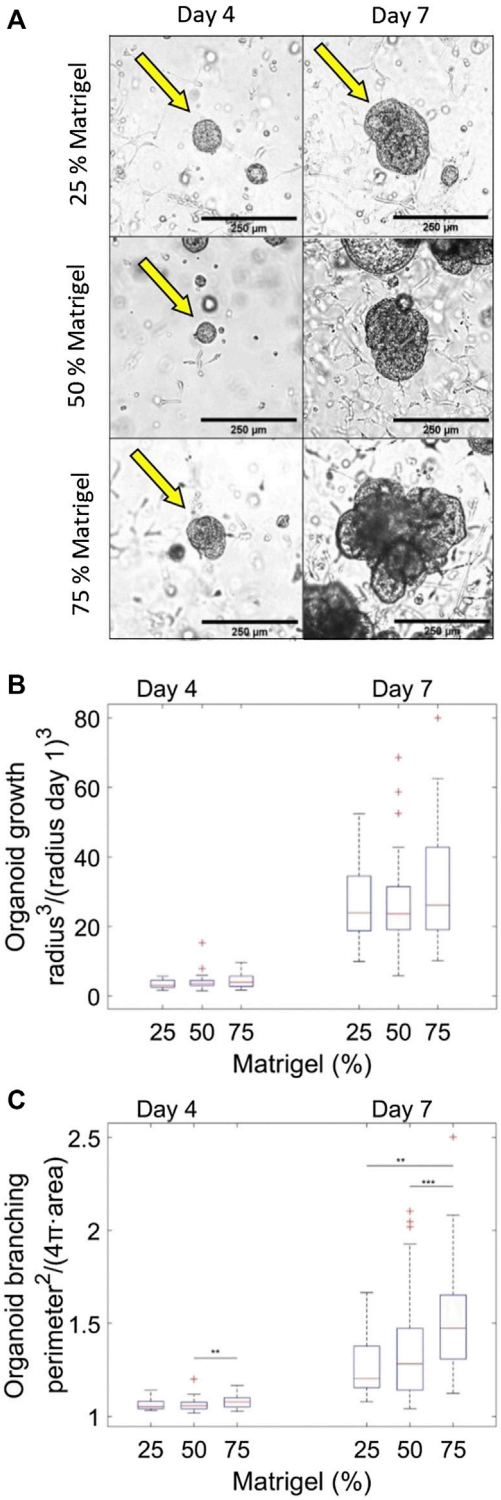

FIGURE 5 | Quantification of organoid branching in Matrigel matrices of different concentrations. **(A)** Representative pictures of organoid growth over time in 75%, 50%, and 25% Matrigel matrices at Day 4 and Day 7, respectively. If more objects are present in an image, arrows point to examples of organoids used for data analysis. **(B)** Quantification of organoid growth in Matrigel matrices with different concentrations (25%, 50%, 75%).

(*Continued*)

that is, independent of the overall size or the organoid, the perimeter^2/area ratio, which is dimensionless, was calculated for each organoid at each Matrigel concentrations at day 4 and at day 7. This ratio was normalized by 4π, which is the value of the ratio for a perfect disk. Hence, the measure depicted in **Figure 5C**) is perimeter^2/area for an organoid divided by the same ratio for a disk. If the measure exceeds 1, the organoid has some degree of branching. This measure of branching is plotted in **Figure 5C**) as a function of time elapsed since seeding of the organoids in the Matrigel matrix. Notice that even at the first time point (D4), the elastic properties of the matrix have reached their static behavior (cf **Figure 2B**).

D'Agostino tests performed on the distributions shown in **Figure 5C** showed that a fair fraction of the distributions were not normally distributed. Hence, to evaluate whether the distributions were statistically significantly different, Mann-Whitney U tests were performed. At day 4 after seeding, organoids embedded in Matrigel matrices at all tested concentrations showed minimal branching with an average normalized perimeter^2/(4πarea) value between 1.06 and 1.08. At this early developmental stage there is, however, already significantly more branching in the 75% Matrigel concentration than in the 50% Matrigel concentration (p = 5.7e-3). At day 7, organoids embedded in the 75% Matrigel matrix have visibly and statistically significantly more branching than those embedded in the 50% (p = 2.9e-04) and the 25% Matrigel matrices (p = 1.8e-3). The average values of normalized perimeter^2/(4πarea) at day 7 for the 25%, 50%, and 75% Matrigel concentrations are 1.27 ± 0.17, 1.36 ± 0.27, and 1.53 ± 0.29, respectively, with median values of 1.20 interquartile range (IQR) 0.22, 1.28 IQR 0.33, and 1.47 IQR 0.34, respectively.

These results show a correlation between the biophysical properties of the medium that organoids are seeded in and the developing morphology of organoids. When the Matrigel concentration is higher, the matrix becomes stiffer, as measured both by the power spectral method and through shear- and storage moduli. A higher degree of branching during pancreas organoid growth is observed for matrices of higher stiffness.

While one may have expected that the stiffness of the environment may either promote growth [41] or limit it by its resistance to compression, this was not observed in the range tested. Instead, the more rigid matrix affects the degree of organoid branching, with more branching observed at higher

FIGURE 5 | The organoid growth is monitored over time. The average of the normalized volumes r/(r Day 1) and the standard deviations are plotted for each condition and each time point. n = 12, 33, and 29 organoids grown in 25%, 50%, and 75% Matrigel, respectively, distributed in two independent experimental repeats. **(C)** Effect of Matrigel concentration on branching quantified by the dimensionless measure: Normalized perimeter^2/area which is plotted as a function of time and for different Matrigel concentrations (25%, 50%, and 75%). At Day 7, there is a significant increase in branching as the Matrigel concentration is increased. n = 12, 66, and 49 organoids for 25%, 50%, and 75% Matrigel, respectively, distributed in two independent experimental repeats.

Matrigel concentrations. It is possible that when an organoid has penetrated a certain region of a rigid medium, the organoid expands more easily at this position and hence creates branches here. More of the organoid's growth will then appear at this position compared to the case of a less rigid growth medium where a more uniform expansion is easier. This may be alike what was reported during the formation of cortical gyri where a mechanical instability due to tangential expansion of cells has non-linear consequences [42].

CONCLUSION

Optical tweezers-based micro-rheology provides a simple method to quantify visco-elastic properties in a highly localized manner and potentially deep within a sample over a large frequency range. Here, we tracked thermal fluctuations of tracer particles inside Matrigel solutions while systematically varying polymer concentrations. This allowed for extraction of the visco-elastic properties of the polymer matrix at different polymer concentrations; the visco-elastic properties were quantified though the scaling properties of the tracer particle's positional power spectrum and by calculating the complex shear moduli.

The visco-elastic properties of a Matrigel-based polymer matrix were found to be highly dependent on polymer concentration, the higher the polymer concentration, the more elastic (less viscous) the matrix. Also, we found that the visco-elastic properties of the Matrigel matrix change over time, with the matrix being more viscous when it is first made and after a few hours it becomes more elastic and settles to a permanent degree of elasticity.

Organoids embedded in a higher Matrigel concentration developed a larger degree of branching, however, their overall size did not change with Matrigel concentration. Being aware of the fact that organoid growth morphology is dependent on Matrigel concentration will be important for bioengineering of proper growth matrices and for understanding how tissues mechanically interact with their environment.

DATA AVAILABILITY STATEMENT

The raw data supporting the conclusions of this article will be made available by the authors, without undue reservation.

AUTHOR CONTRIBUTIONS

The study was designed by LBO, MB, YFB, KBS and AGB. The experimental data was acquired and analyzed by MB, YFB and SY. All authors discussed all results and participated in writing the manuscript.

ACKNOWLEDGMENTS

The authors acknowledge financial support from the Danish National Research Council, grant number DNRF116. The Novo Nordisk Foundation Center for Stem Cell Biology is supported by a Novo Nordisk Foundation grant number NNF17CC0027852.

REFERENCES

1. Lo CM, Wang HB, Dembo M, Wang YL. Cell movement is guided by the rigidity of the substrate. *Biophys J* (2000) **79**:144–52. doi:10.1016/S0006-3495(00)76279-5
2. Kim MC, Silberberg YR, Abeyaratne R, Kamm RD, Asada HH. Computational modeling of three-dimensional ECM-rigidity sensing to guide directed cell migration. *Proc Natl Acad Sci USA* (2018) **115**:E390–9. doi:10.1073/pnas.1717230115
3. Wells RG. The role of matrix stiffness in regulating cell behavior. *Hepatology* (2008) **47**:1394–400. doi:10.1002/hep.22193
4. Shin JW, Mooney DJ. Extracellular matrix stiffness causes systematic variations in proliferation and chemosensitivity in myeloid leukemias. *Proc Natl Acad Sci USA* (2016) **113**:12126–31. doi:10.1073/pnas.1611338113
5. Cavo M, Fato M, Peñuela L, Beltrame F, Raiteri R, Scaglione S. Microenvironment complexity and matrix stiffness regulate breast cancer cell activity in a 3D *in vitro* model. *Sci Rep* (2016) **6**, 35367. doi:10.1038/srep35367
6. Smith LR, Cho S, Discher DE. Stem cell differentiation is regulated by extracellular matrix mechanics. *Physiology* (2018) **33**:16–25. doi:10.1152/physiol.00026.2017
7. Hwang JH, Byun MR, Kim AR, Kim KM, Cho HJ, Lee YH, et al. Extracellular matrix stiffness regulates osteogenic differentiation through MAPK activation. *PLoS One* (2015) **10**:1–16. doi:10.1371/journal.pone.0135519
8. Olsen AL, Bloomer SA, Chan EP, Gaça MDA, Georges PC, Sackey B, et al. Hepatic stellate cells require a stiff environment for myofibroblastic differentiation. *Am J Physiol Gastrointest Liver Physiol* (2011) **301**:G110–8. doi:10.1152/ajpgi.00412.2010
9. Wullkopf L, West AKV, Leijnse N, Cox TR, Madsen CD, Oddershede LB, et al. Cancer cells' ability to mechanically adjust to extracellular matrix stiffness correlates with their invasive potential. *Mol Biol Cell* (2018) **29**:2378–85. doi:10.1091/mbc.E18-05-0319
10. Bordeleau F, Mason BN, Lollis EM, Mazzola M, Zanotelli MR, Somasegar S, et al. Matrix stiffening promotes a tumor vasculature phenotype. *Proc Natl Acad Sci USA* (2017) **114**:492–7. doi:10.1073/pnas.1613855114
11. Soofi SS, Last JA, Liliensiek SJ, Nealey PF, Murphy CJ. The elastic modulus of matrigel$_{TM}$ as determined by atomic force microscopy. *J Struct Biol* (2009) **167**:216–9. doi:10.1016/j.jsb.2009.05.005
12. Koutsopoulos S, Zhang S. Long-term three-dimensional neural tissue cultures in functionalized self-assembling peptide hydrogels, matrigel and collagen I. *Acta Biomater* (2013) **9**:5162–9. doi:10.1016/j.actbio.2012.09.010
13. Tolić-Nørrelykke IM, Munteanu EL, Thon G, Oddershede L, Berg-Sørensen K. Anomalous diffusion in living yeast cells. *Phys Rev Lett* (2004) **93**:078102. doi:10.1103/PhysRevLett.93.078102
14. Wessel A, Maheshwar G, Grosshans J, Schmidt C. The mechanical properties of early drosophila embryos measured by high-speed video microrheology. *Biophys J* (2015) **108**:1899–1907. doi:10.1016/j.bpj.2015.02.032
15. MacKintosh F, Kas J, Janmey P. Elasticity of semiflexible biopolymer networks. *Phys Rev Lett* (1995) **75**:4425–8. doi:10.1103/PhysRevLett.75.4425
16. Greggio C, De Franceschi F, Figueiredo-Larsen M, Grapin-Botton A. *In vitro* pancreas organogenesis from dispersed mouse embryonic progenitors. *J Vis Exp* (2014) (89):51725. doi:10.3791/51725
17. Greggio C, De Franceschi F, Grapin-Botton A. Concise reviews: in vitro-produced pancreas organogenesis models in three dimensions: self-organization from few stem cells or progenitors. *Stem Cell* (2015) **33**:8–14. doi:10.1002/stem.1828

18. Gittes F, Schmidt CF. Interference model for back-focal-plane displacement detection in optical tweezers. *Opt lett* (1998) **23**:7–9. doi:10.1364/ol.23.000007
19. Allersma MW, Gittes F, DeCastro MJ, Stewart RJ, Schmidt CF. Two-dimensional tracking of ncd motility by back focal plane interferometry. *Biophys J* (1998) **74**:1074–85. doi:10.1016/S0006-3495(98)74031-7
20. Rohrbach A. Stiffness of optical traps: quantitative agreement between experiment and electromagnetic theory. *Phys Rev Lett* (2005) **95**:168102. doi:10.1103/PhysRevLett.95.168102
21. Svoboda K, Block SM. Biological applications of optical forces. *Annu Rev Biophys Biomol Struct* (1994) **23**:247–85. doi:10.1146/annurev.bb.23.060194.001335
22. Gittes F, Schmidt CF. Signals and noise in micromechanical measurements. *Methods Cell Biol* (1998) **55**:129–56. doi:10.1016/S0091-679X(08)60406-9
23. Schnurr B, Gittes F, MacKintosh F, Schmidt C. Determining microscopic viscoelasticity in flexible and semiflexible polymer networks from thermal fluctuations. *Macromolecules* (1997) **30**:7781–92. doi:10.1021/MA970555N
24. Pesce G, De Luca AC, Rusciano G, Netti PA, Fusco S, Sasso A. Microrheology of complex fluids using optical tweezers: a comparison with macrorheological measurements. *J Opt A Pure Appl Opt* (2009) **11**:034016. doi:10.1088/1464-4258/11/3/034016
25. Mizuno D, Head DA, MacKintosh FC, Schmidt CF. Active and passive microrheology in equilibrium and nonequilibrium systems. *Macromolecules* (2008) **41**:7194–202. doi:10.1021/ma801218z
26. Berg-Sørensen K, Oddershede L, Florin EL, Flyvbjerg H. Unintended filtering in a typical photodiode detection system for optical tweezers. *J Appl Phys* (2003) **93**:3167–76. doi:10.1063/1.1554755
27. Xing Q, Qian Z, Jia W, Ghosh A, Tahtinen M, Zhao F. Natural extracellular matrix for cellular and tissue biomanufacturing. *ACS Biomater Sci Eng* (2016) **3**:1462–76. doi:10.1021/acsbiomaterials.6b00235
28. Uriel S, Labay E, Francis-Sedlak M, Moya ML, Weichselbaum RR, Ervin N, et al. Extraction and assembly of tissue-derived gels for cell culture and tissue engineering. *Tissue Eng C* (2009) **15**:309–21. doi:10.1089/ten.tec.2008.0309
29. Francis MP, Sachs PC, Madurantakam PA, Sell SA, Elmore LW, Bowlin GL, et al. Electrospinning adipose tissue-derived extracellular matrix for adipose stem cell culture. *J Biomed Mater Res* (2012) **100A**:1716–24. doi:10.1002/jbm.a.34126
30. Lin M, Jingwu L, Qiang N, Qiuyang Z, Qiuyang Z, Sen L, et al. Organoid culture of human prostate cancer cell lines LNCaP and C4-2B. *Am J Clin Exp Urol* (2017) **5**:25–33. doi:10.1002/ijc.33315
31. Molina-Jimenez F, Benedicto I, Thi VLD, Gondar V, Lavillette D, Marin JJ, et al. Matrigel-embedded 3D culture of huh-7 cells as a hepatocyte-like polarized system to study hepatitis C virus cycle. *Virology* (2012) **425**:31–9. doi:10.1016/j.virol.2011.12.021
32. Drost J, Karthaus WR, Gao D, Driehuis E, Sawyers CL, Chen Y, et al. Organoid culture systems for prostate epithelial and cancer tissue. *Nat Protoc* (2016) **11**: 347–58. doi:10.1038/nprot.2016.006
33. Sodunke TR, Turner KK, Caldwell SA, McBride KW, Reginato MJ, Noh HM. Micropatterns of matrigel for three-dimensional epithelial cultures. *Biomaterials* (2007) **28**:4006–16. doi:10.1016/j.biomaterials.2007.05.021
34. Hughes CS, Postovit LM, Lajoie GA. Matrigel: a complex protein mixture required for optimal growth of cell culture. *Proteomics* (2010) **10**:1886–90. doi:10.1002/pmic.200900758
35. Kuo CT, Wang JY, Lin YF, Wo AM, Chen BPC, Lee H. Three-dimensional spheroid culture targeting versatile tissue bioassays using a PDMS-based hanging drop array. *Sci Rep* (2017) **7**:4363. doi:10.1038/s41598-017-04718-1
36. Anguiano M, Castilla C, Maska M, Ederra C, Pelaez R, Morales X, et al. Characterization of three-dimensional cancer cell migration in mixed collagen-matrigel scaffolds using microfluidics and image analysis. *PLoS One* (2017) **12**:e0171417. doi:10.1371/journal.pone.0171417
37. Cui X, Hartanto Y, Zhang H. Advances in multicellular spheroids formation. *J R Soc Interface* (2017) **14**:20160877. doi:10.1098/rsif.2016.0877
38. Berg-Sørensen K, Flyvbjerg H. Power spectrum analysis for optical tweezers. *Rev Sci Instrum* (2004) **75**:594–612. doi:10.1063/1.1645654
39. Hansen PM, Tolić-Nørrelykke IM, Flyvbjerg H, Berg-Sørensen K. Tweezercalib 2.0: faster version of matlab package for precise calibration of optical tweezers. *Comput Phys Commun* (2006) **174**:518–20. doi:10.1016/j.cpc.2005.11.007
40. Loosemore VE, Forde NR. Effects of finite and discrete sampling and blur on microrheology experiments. *Opt Express* (2017) **25**:31239–52. doi:10.1364/OE.25.031239
41. Gjorevski N, Sachs N, Manfrin A, Giger S, Bragina ME, Ordóñez-Morán P, et al. Designer matrices for intestinal stem cell and organoid culture. *Nature* (2016) **539**:560–4. doi:10.1038/nature20168
42. Tallinen T, Chung J, Biggins J, Mahadevan L. Gyrification from constrained cortical expansion. *Proc Natl Acad Sci USA* (2014) **111**12667–72. doi:10.1073/pnas.1406015111

Conflict of Interest: The authors declare that the research was conducted in the absence of any commercial or financial relationships that could be construed as a potential conflict of interest.